LETTER

Molecular beam epitaxy growth of superconducting LiFeAs film on $SrTiO_3$(001) substrate

To cite this article: K. Chang *et al* 2015 *EPL* **109** 28003

A Letters Journal Exploring the Frontiers of Physics

January 2015

EPL, **109** (2015) 28003 www.epljournal.org
doi: 10.1209/0295-5075/109/28003

Molecular beam epitaxy growth of superconducting LiFeAs film on $SrTiO_3(001)$ substrate

K. Chang[1,2], P. Deng[1,2], T. Zhang[1,2], H.-C. Lin[1,2], K. Zhao[1,2], S.-H. Ji[1,2,3(a)], L.-L. Wang[1,2], K. He[1,2], X.-C. Ma[1,2], X. Chen[1,2(b)] and Q.-K. Xue[1,2(c)]

[1] *State Key Laboratory of Low-Dimensional Quantum Physics, Department of Physics, Tsinghua University Beijing 100084, China*
[2] *Collaborative Innovation Center of Quantum Matter - Beijing 100084, China*
[3] *RIKEN Center for Emergent Matter Science (CEMS) - Wako, Saitama 351-0198, Japan*

received 26 September 2014; accepted in final form 7 January 2015
published online 28 January 2015

PACS 81.15.Hi – Molecular, atomic, ion, and chemical beam epitaxy
PACS 74.70.Xa – Superconducting materials other than cuprates: Pnictides and chalcogenides
PACS 68.37.Ef – Scanning tunneling microscopy (including chemistry induced with STM)

Abstract – The stoichiometric "111" iron-based superconductor, LiFeAs, has attacted great research interest in recent years. For the first time, we have successfully grown a LiFeAs thin film by molecular beam epitaxy (MBE) on a $SrTiO_3(001)$ substrate, and studied the interfacial growth behavior by reflection high-energy electron diffraction (RHEED) and low-temperature scanning tunneling microscope (LT-STM). The effects of substrate temperature and Li/Fe flux ratio were investigated. A uniform LiFeAs film as thin as 3 quintuple layers (QL) is formed. A superconducting gap appears in LiFeAs films thicker than 4 QL at 4.7 K. When the film is thicker than 13 QL, the superconducting gap determined by the distance between the coherence peaks is about 7 meV, close to the value of bulk material. The *ex situ* transport measurement of a thick LiFeAs film shows a sharp superconducting transition around 16 K. The upper critical field, $H_{c2}(0) = 13.0$ T, is estimated from the temperature-dependent magnetoresistance. The precise thickness and quality control of the LiFeAs film paves the road for growing similar ultrathin iron arsenide films.

Introduction. – LiFeAs is a "111" type iron-based superconductor (Fe-SC) and has recently attracted much attention due to its unusual properties compared to other superconducting iron pnictides. Without chemical doping, the stoichiometric LiFeAs already shows a superconducting transition at 18 K under the ambient pressure [1–3]. More interestingly, the magnetic structure driven by the Fermi surface nesting between electron-like and hole-like pockets, an essential ingredient for the parent compound of iron pnictide superconductors, is absent in LiFeAs [4–7]. Both $s_{\pm}$-wave singlet and p-wave triplet pairings have been proposed for LiFeAs [8,9].

LiFeAs has a layered tetragonal structure ($p4/nmm$). As shown in fig. 1(a), an edge-sharing $FeAs_4$-tetrahedra layer in LiFeAs consists of one layer of Fe sandwiched between two layers of As. Compared with the square lattice formed by the Fe atoms, the lattice of As atoms rotates by 45° and enlarges by a factor of $\sqrt{2}$ [1–3]. Two layers of Li atoms are intercalated between FeAs and form the neutral cleaving plane without surface reconstruction. Therefore, the surface sensitive probes, such as scanning tunneling microscope (STM) and angle-resolved photoelectron spectroscopy (ARPES), have been successfully applied to capture the intrinsic properties of LiFeAs [4,5,10–13].

The synthesis of a high-quality single crystal is critical for a comprehensive study of LiFeAs. Similar to some other iron pnictides, LiFeAs was first synthesized by the high-pressure method [1–3]. The flux and self-flux methods have also been introduced to produce a larger-size single crystal up to a millimeter [14,15]. There has been no LiFeAs film grown by MBE, a powerful method to grow single-crystal thin films up to the centimeter scale, till now. Although several other iron arsenide

(a) E-mail: shji@mail.tsinghua.edu.cn
(b) E-mail: xc@mail.tsinghua.edu.cn
(c) E-mail: qkxue@mail.tsinghua.edu.cn

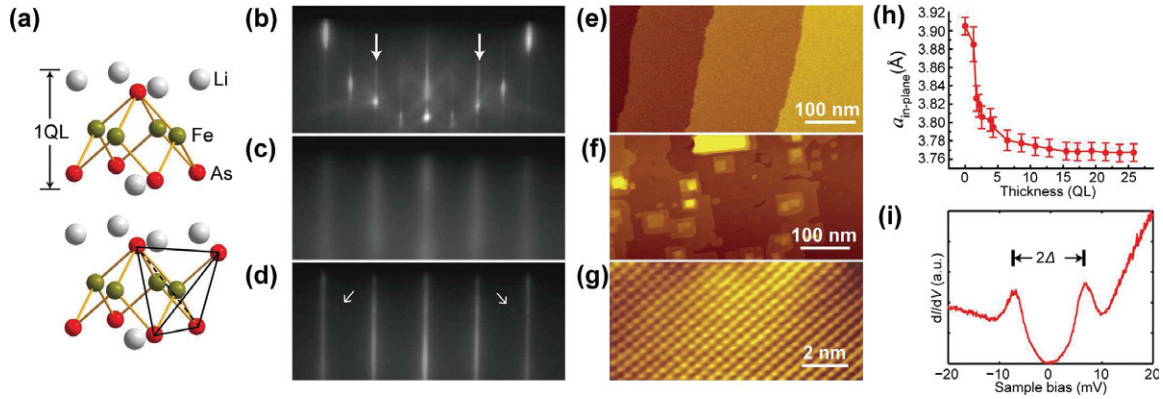

Fig. 1: (Color online) MBE growth of LiFeAs film. (a) The tetragonal structure of LiFeAs. (b) RHEED pattern of the (001) surface of the $SrTiO_3$ substrate, which shows the 2×2 reconstruction. The arrows indicate the 1×1 stripes. (c), (d): RHEED patterns of a LiFeAs thin film on the $SrTiO_3$ substrate after 8 (c) and 60 (d) minutes deposition. The weak spots marked by the arrows show the formation of a small amount of Li_3As clusters on the surface during growth. (e), (f): STM topographic images of $SrTiO_3(001)$ (e) and 25 QL LiFeAs film (f). Image size: 500 nm × 250 nm; sample bias: 1.0 V; tunneling current: 100 pA. (g) Atomically resolved STM topography image on the surface of a 25 QL LiFeAs film (10 nm × 10 nm, 8.0 mV, 2.0 nA). (h) The evolution of the in-plane lattice constant $a_{\text{in-plane}}$ determined by RHEED as a function of the film thickness. (i) The dI/dV spectrum on the surface of a 13 QL LiFeAs film.

superconductors have been grown by MBE [16–19], those films were all thicker than 100 nm and the interfacial behavior has never been studied. In order to achieve thickness control with atomic precision, we performed the epitaxial growth of LiFeAs single-crystal thin films on the $SrTiO_3(001)$ surface. The superconductivity in the LiFeAs film is then characterized by STM and transport measurement.

Experimental method. – The experiment was carried out on a Unisoku low-temperature STM combined with MBE. The base pressure is lower than 1×10^{-10} torr. The LiFeAs films were grown in the MBE chamber and immediately transferred into the STM at a temperature of 4.7 K without taking out of the ultra-high vacuum (UHV) environment. A PtIr alloy tip was used in STM for topography and spectroscopy measurement.

The Nb-doped $SrTiO_3(001)$ substrate was cleaned in UHV by direct current heating up to 1200 °C for several times. Each time the heating lasted for 5 minutes. The temperature of the substrate was monitored by an infrared pyrometer. Li and Fe were evaporated from two standard Knudsen cells (K-cell). The evaporation temperatures were around 400 °C and 1100 °C, respectively. In the conventional MBE growth of arsenide, As flux is obtained by directly heating solid As, producing As_2 and As_4 molecules with low reactivity. In order to obtain more reactive atomic As, we used the FeAs compound with high purity as the source for As. The FeAs compound was heated to ∼ 400 °C in K-cell and decomposed into atomic Fe and As. Due to the huge vapor pressure difference between As (10^{-4} torr at 200 °C) and Fe (10^{-4} torr at 1220 °C), the flux consists of nearly pure As atoms, which was confirmed by quadruple mass spectrometer. During the epitaxial growth, the flux of As was much higher than that of Fe (flux ratio $> 20 : 1$). The flux ratio between Fe and Li was finely tuned to prevent the formation of Li_3As or FeAs, which shows additional spots in the RHEED pattern. A Sigma Q-pod crystal oscillator measured the flux of Fe. The growth rate of LiFeAs films is approximately 0.2–0.4 quintuple layers (QL, one LiFeAs unit cell) per minute, depending on the temperature of the Fe source.

The transport measurements were carried out *ex situ* on a Quantum Design PPMS system, where the lowest temperature is 1.8 K and the highest magnetic field is 9 T. To avoid the degrading of LiFeAs film in the ambient atmosphere, a several-nanometer–thick Ag protection layer was deposited on the top of the LiFeAs epitaxial film before taking out of UHV.

Results and discussion. – The sharp patterns and Kikuchi lines of the reflection high-energy electron diffraction (RHEED) in fig. 1(b) show the cleanness and flatness of the $SrTiO_3$ substrate after high-temperature treatment in UHV. Besides the 1×1 pattern for the (001) surface along the ⟨010⟩ direction (indicated by the arrows in fig. 1(b)), the lines between the 1×1 streaks show the 2×2 reconstruction of the surface.

450 °C is the optimal substrate temperature to achieve layer-by-layer growth of LiFeAs on $SrTiO_3$. Upon growth, the RHEED pattern of the substrate disappeared quickly and then a much more broadened 1×1 pattern (fig. 1(c)) appeared with the same orientation as the substrate, indicating the coherent epitaxial nature of the growth. As the deposition time increases, the RHEED pattern becomes sharper. No RHEED intensity oscillation has been observed. Figure 1(d) shows the 1×1 RHEED pattern of a 25 QL LiFeAs. The single-crystalline nature of the thin film was further verified by the RHEED patterns with different substrate azimuth.

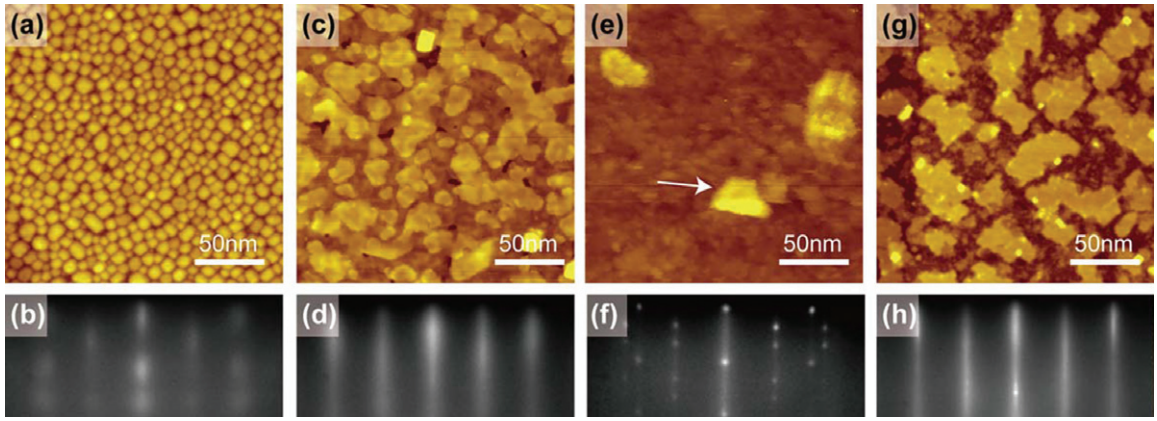

Fig. 2: (Color online) Evolution of topography and RHEED pattern with different Li flux and substrate temperature. (a)–(f) STM images and RHEED of LiFeAs films grown at 345 °C substrate temperature with the same Fe flux. The Li source temperatures are 374 °C ((a), (b)), 390 °C ((c), (d)) and 400 °C ((e), (f)), respectively. The arrow in (e) indicates a triangular Li_3As island. (g), (h): STM image and RHEED of a sample grown at 450 °C substrate temperature. All the fluxes are the same as (e). Image conditions for all STM images: 3.0 V and 30 pA.

The very weak spots marked by the arrows in fig. 1(d) are attributed to a small amount of Li_3As clusters on the surface of the film, which is introduced by slightly excessive Li flux. The superconductivity of LiFeAs films is not significantly influenced by these Li_3As clusters (however, excessive Fe flux does severely suppress superconductivity). With careful tuning of the Li flux, the extra spots can be completely removed.

In the STM image of the substrate (fig. 1(e)), the average terrace width is up to several hundred nanometers. The step height of 3.9 Å corresponds to one unit cell of $SrTiO_3$. The image in fig. 1(f) reveals the atomically flat surface of an epitaxial 25 QL LiFeAs film on $SrTiO_3$ and the flat area size can be up to 100 nm. The atomic step height 6.3 Å, measured from the STM image, corresponds to one QL of LiFeAs. In addition, rectangular islands and screw dislocations are visible on the terraces.

The atomically resolved image (fig. 1(g)) shows the square lattice with an atomic spacing of 3.8 Å, which is consistent with the lattice constant of LiFeAs(001) [10–13]. Similar to the cleaved (001) surface, no surface reconstruction has been observed on the epitaxial LiFeAs thin film. We believe that the surface is terminated by Li instead of As since the As-terminated surface normally has reconstruction for the iron pnictide superconductor [20]. The thickness dependence of the lattice constant is estimated from the RHEED pattern and shown in fig. 1(h). The in-plane lattice constant of the LiFeAs thin film continuously decreases from 3.91 Å, the lattice constant of the $SrTiO_3$ substrate, to 3.77 Å, that of the LiFeAs bulk material. The curve in fig. 1(h) shows that the lattice of the first few epitaxial layers expands due to the lattice mismatch between LiFeAs and $SrTiO_3$ substrate. The lattice of the film relaxes to that of the bulk material within 15 QL. A well-defined superconducting gap with sharp coherence peaks is revealed by scanning tunneling spectroscopy (STS) on a film thicker than 13 QL (fig. 1(i)). The gap size $\Delta \sim 7$ meV is consistent with the previous reports on bulk materials [10,11,13].

Li/Fe flux ratio is essential for LiFeAs film growth. Figures 2(a)–(f) illustrate three samples grown under the same Fe flux and substrate temperature (345 °C), but with different Li flux. The nominal thickness of the samples is 3 QL. When Li is insufficient, small islands of several nanometers appear (fig. 2(a)) and the RHEED pattern (fig. 2(b)) exhibits dim spots. If the Li flux is increased to a certain value, a continuous film (fig. 2(c)) with high density of screw dislocations is formed. The RHEED pattern (fig. 2(d)) shows stripes corresponding to the LiFeAs lattice constant 3.8 Å. A further increase of the Li flux leads to triangular islands on the film (fig. 2(e)). In the RHEED pattern (fig. 2(f)), a set of sharp spots superposes on the LiFeAs stripe. The analysis shows that the spots correspond to these triangular Li_3As islands on the surface.

Besides the Li/Fe flux ratio, the substrate temperature is another important factor to determine the film topography. In particular, the effective Li flux changes with the substrate temperature because of the desorption of Li atoms, which is more pronounced when the Li source temperature (usually 350–400 °C) is close to that of the substrate. For example, the sample in fig. 2(g) was grown under the same flux of Li, Fe and As as that in fig. 2(e), but with the substrate temperature raised to 450 °C. There is no longer Li_3As islands on the film and the RHEED shows a similar pattern as that in fig. 2(d) without the sharp spots. Therefore, the Li source temperature has to be adjusted for each substrate temperature to maintain effectively the same Li/Fe flux ratio.

By adjusting the Li/Fe flux ratio at the optimal substrate temperature (450 °C), we can obtain an atomically flat film as thin as ∼3 QL. Below 3 QL, LiFeAs islands with a several-tens-of-nanometer lateral size are formed (figs. 3(a) and (b)). The atom-resolved image on

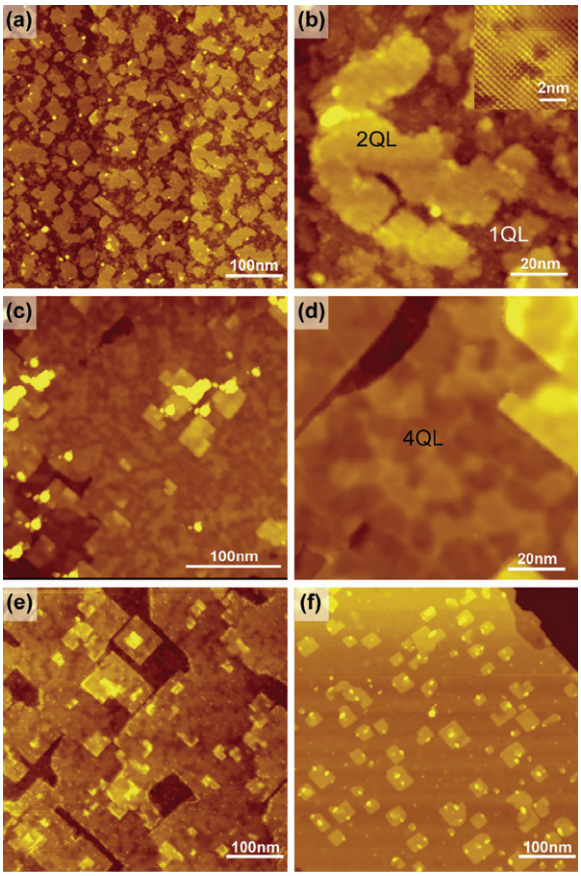

Fig. 3: (Color online) STM topography of LiFeAs films with various thicknesses. The temperature of substrate was fixed at 450 °C during growth. (a) 1.5 QL (500 nm × 500 nm, 3.0 V, 30 pA). (b) Detailed features of the film in (a) (100 nm × 100 nm, 2.0 V, 50 pA). Inset: the atom-resolved image obtained from a 2 QL island (8 nm × 8 nm, 50 mV, 100 pA). (c) 4.5 QL (300 nm × 300 nm, 3.0 V, 30 pA). (d) Detailed features of the film in (c) (100 nm × 100 nm, 1.0 V, 80 pA). (e) 7.5 QL (500 nm × 500 nm, 3.5 V, 25 pA). (f) 13 QL (500 nm × 500 nm, 4.0 V, 30 pA).

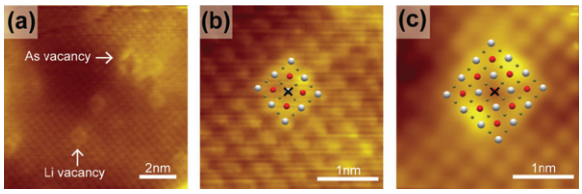

Fig. 4: (Color online) Defects in LiFeAs film. (a) Image showing Li and As vacancies. 5.0 mV, 1.0 nA. (b) A Li vacancy. 5.0 mV, 1.0 nA. (c) An As vacancy. 8.0 mV, 0.4 nA. The lattice model of LiFeAs is superposed on the images. White, red and grey balls stand for the topmost Li, As and Fe atoms, respectively. The vacancy is indicated by a cross.

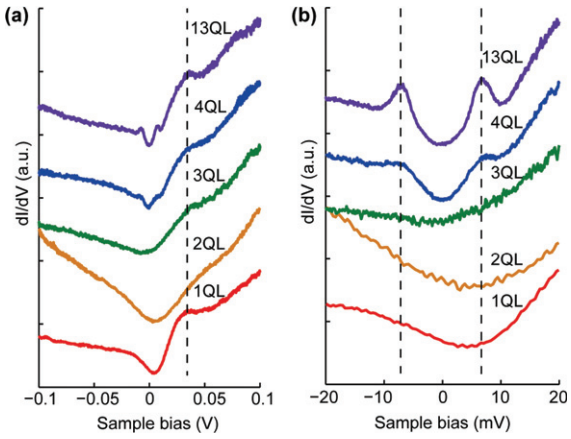

Fig. 5: (Color online) Thickness dependence of the dI/dV spectra: (a) from −0.1 V to 0.1 V and (b) from −20 mV to 20 mV. The spectra are vertically shifted for clarity. The superconducting gap begins to emerge when thickness is 4 QL. The dashed line in (a) indicates the kink at 36 meV, which was also seen in the cleaved LiFeAs single crystals. The dashed lines in (b) label the coherence peaks.

a 2 QL island shows the square lattice constant of 3.85 Å, consistent with the RHEED data (fig. 3(b), inset). The dI/dV spectra measured off the islands are identical to that of the $SrTiO_3$ substrate, confirming the island thickness assignment. On $SrTiO_3$, it is difficult to follow the layer-by-layer growth mode, mainly because Li tends to form clusters on the substrate. The thicker film becomes flatter and more uniform (fig. 3(c)). Screw dislocations appear on the surface, probably originating from the merging of islands. We note that the density of screw dislocation in the film grown at 450 °C is much lower than that grown at 350 °C. The surface corrugation of a 4 QL film (fig. 3(d)) is about 2 Å, which may be attributed to the unreleased strain induced by the substrate. When the film thickness increases to 7.5 QL, single QL islands appear on the surface (fig. 3(e)). Above 13 QL (fig. 3(f)), there are very few screw dislocations and very low surface corrugation, implying that the strain has been sufficiently released. The strain relief is also indicated by the lattice constant measured from RHEED patterns (fig. 1(h)).

Two types of defects are visible on the surface (fig. 4(a)). The Li vacancy (fig. 4(b)) appears as a hole in the topmost layer. The eight neighboring Li atoms are brighter in the STM image. The larger defect (fig. 4(c)) can be ascribed to the As vacancy in the second layer. An As atom sits in the center of four Li atoms, and both the nearest and the next-to-nearest Li atoms in the topmost layer are influenced by the absence of an As atom. Interestingly, the Fe vacancies with 2-fold symmetry, which are frequently seen in the cleaved bulk materials [21], are seldom seen in the MBE film. In the MBE growth, the relatively low substrate temperature prevents the generation of Fe vacancies. For comparison, the synthesis temperature for the LiFeAs single crystal is usually as high as 800 °C [1].

We performed STS measurements on the films with different thicknesses (fig. 5). A superconducting gap at the Fermi level begins to emerge when the thickness is 4 QL. The 13 QL film shows a gap with pronounced coherence

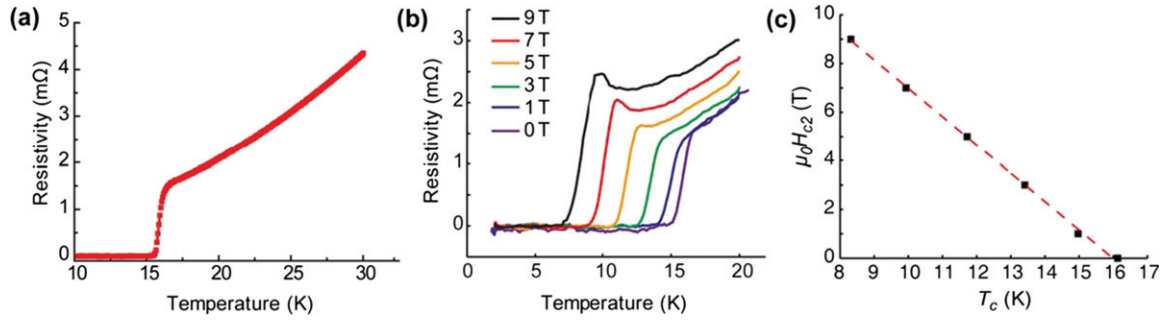

Fig. 6: (Color online) (a) Temperature dependence of resistivity of a ∼100 QL LiFeAs film with silver capping layer under zero magnetic field. It shows a superconducting transition temperature $T_c = 16$ K. (b) Magnetoresistance measured under the field perpendicular to the film from 0 T to 9 T. (c) Magnetic-field dependence of the superconducting transition temperature T_c. The linear fitting gives the slope $\mathrm{d}H_{c2}/\mathrm{d}T = -1.17$ T/K, corresponding to the critical field $H_{c2} = 13.0$ T at zero temperature.

peaks. The peak-to-peak distance is $2\Delta \sim 14$ meV. The $\mathrm{d}I/\mathrm{d}V$ spectrum of the film is consistent with that of the bulk materials [13], including the kink at 36 meV (fig. 5(a), indicated by dashed line). Superconductivity is absent in a film thinner than 4 QL at liquid-helium temperature.

There are several possible reasons to account for this superconductivity degrading in the LiFeAs thin film. The first one is the size effect, *i.e.*, the superconducting transition temperature of the thin film is suppressed as the thickness is reduced down to the coherence length scale. This effect has been reported for several superconductors with atomic-layer thickness [22–24]. The second possible reason is the tensile strain imposed by the substrate, which could not be excluded in our case because the transition temperature of iron-based superconductors is sensitive to the lattice constant change [25–27]. From a 4 QL to a 3 QL film, the superconducting gap drops abruptly to zero at liquid-helium temperature. It is likely attributed to the sharp change of the in-plane lattice constant which is clearly revealed in fig. 1(h). The third reason which needs to be considered is that the electronic or magnetic structure of a very thin LiFeAs film may be modulated by the substrate, which has already been observed in the epitaxial FeSe film on the $SrTiO_3(001)$ surface [28–30]. All these effects could also be entangled and further theoretical work is needed to fully explain the behaviors observed in our LiFeAs thin film.

Furthermore, we measured the transport properties of the LiFeAs thin film. Since LiFeAs degrades in the ambient atmosphere, several-nanometer–thick silver was deposited on top of LiFeAs as the protection layer before the sample was taken out of UHV for transport measurement. Figure 6(a) shows the temperature dependence of resistance for a 100 QL LiFeAs film with silver capping layer. The sharp superconducting transition occurs at 16 K, which is close to the bulk value of 18 K [1–3]. Figure 6(b) shows the magnetoresistance with magnetic field perpendicular to the sample. The superconducting transition shifts to lower temperature as the magnetic field increases from 0 T to 9 T. At the same time the normal state resistance increases. The magnetic-field dependence of T_c (fig. 6(c)) is almost linear between 0 T and 9 T. A linear fitting gives the slope $\mu_0 \mathrm{d}H_{c2}/\mathrm{d}T = -1.17$ T/K. Calculating from the Werthamer-Helfand-Hohenberg formula $\mu_0 H_{c2}(0) = -0.693 \frac{\mu_0 \mathrm{d}H_{c2}(T)}{\mathrm{d}T}|_{T_c} T_c$ [31], the upper critical field at zero temperature is 13.0 T, slightly lower than the bulk value 17 T [32]. For a LiFeAs film thinner than ∼50 QL, it is difficult to detect the superconducting transition since the film is unstable in atmosphere even with the silver capping layer.

Conclusion. – We have realized the molecular beam epitaxial growth of a LiFeAs thin film with high quality on a $SrTiO_3(001)$ substrate. The MBE film makes it possible to study the intrinsic properties of LiFeAs. At 4.7 K, the superconducting gap is revealed in an ultrathin film thicker than 4 QL. The gap size of the 13 QL film is as large as 7 meV, which is close to the bulk value. The 100 QL film shows sharp superconducting transition at 16 K in the transport measurement. The upper critical field H_{c2} is estimated to be 13.0 T from the magnetoresistance measurement. The current growth approach can be applied to other materials consisting of highly reactive alkaline elements, such as NaFeAs and KFe_2As_2. Our work paves the way for further studies on the intrinsic properties of LiFeAs, which can be disturbed by the impurities introduced in the bulk growth methods.

* * *

The authors thank C. Q. Jin for synthesizing the FeAs compound. The work was financially supported by Ministry of Science and Technology of China under grant No. 2013CB934600, National Science Foundation (grant No. 11274151) and Ministry of Education of China.

REFERENCES

[1] Wang X. C., Liu Q. Q., Lv Y. X., Gao W. B., Yang L. X., Yu R. C., Li F. Y. and Jin C. Q., *Solid State Commun.*, **148** (2008) 538.

[2] Tapp J. H., Tang Z., Lv B., Sasmal K., Lorenz B., Chu P. C. W. and Guloy A. M., *Phys. Rev. B*, **78** (2008) 060505.

[3] Pitcher M. J., Parker D. R., Adamson P., Herkelrath S. J. C., Boothroyd A. T., Ibberson R. M., Brunelli M. and Clarke S. J., *Chem. Commun.* (2008) 5918.

[4] Borisenko S. V., Zabolotnyy V. B., Evtushinsky D. V., Kim T. K., Morozov I. V., Yaresko A. N., Kordyuk A. A., Behr G., Vasiliev A., Follath R. and Büchner B., *Phys. Rev. Lett.*, **105** (2010) 067002.

[5] Umezawa K., Li Y., Miao H., Nakayama K., Liu Z. H., Richard P., Sato T., He J. B., Wang D. M., Chen G. F., Ding H. and Takahashi T., *Phys. Rev. Lett.*, **108** (2012) 037002.

[6] Nowik I. and Felner I., *Physica C*, **469** (2009) 485.

[7] Qureshi N., Steffens P., Drees Y., Komarek A. C., Lamago D., Sidis Y., Harnagea L., Grafe H. J., Wurmehl S., Büchner B. and Braden M., *Phys. Rev. Lett.*, **108** (2012) 117001.

[8] Platt C., Thomale R. and Hanke W., *Phys. Rev. B*, **84** (2011) 235121.

[9] Brydon P. M. R., Daghofer M., Timm C. and van den Brink J., *Phys. Rev. B*, **83** (2011) 060501.

[10] Allan M. P., Rost A. W., Mackenzie A. P., Xie Y., Davis J. C., Kihou K., Lee C. H., Iyo A., Eisaki H. and Chuang T. M., *Science*, **336** (2012) 563.

[11] Chi S., Grothe S., Liang R., Dosanjh P., Hardy W. N., Burke S. A., Bonn D. A. and Pennec Y., *Phys. Rev. Lett.*, **109** (2012) 087002.

[12] Hänke T., Sykora S., Schlegel R., Baumann D., Harnagea L., Wurmehl S., Daghofer M., Büchner B., van den Brink J. and Hess C., *Phys. Rev. Lett.*, **108** (2012) 127001.

[13] Hanaguri T., Kitagawa K., Matsubayashi K., Mazaki Y., Uwatoko Y. and Takagi H., *Phys. Rev. B*, **85** (2012) 214505.

[14] Song Y. J., Ghim J. S., Min B. H., Kwon Y. S., Jung M. H. and Rhyee J.-S., *Appl. Phys. Lett.*, **96** (2010) 212508.

[15] Morozov I., Boltalin A., Volkova O., Vasiliev A., Kataeva O., Stockert U., Abdel-Hafiez M., Bombor D., Bachmann A., Harnagea L., Fuchs M., Grafe H.-J., Behr G., Klingeler R., Borisenko S., Hess C., Wurmehl S. and Büchner B., *Cryst. Growth Des.*, **10** (2010) 4428.

[16] Agatsuma S., Yamagishi T., Takeda S. and Naito M., *Physica C*, **470** (2010) 1068.

[17] Ueda S., Yamagishi T., Takeda S., Agatsuma S., Takano S., Mitsuda A. and Naito M., *Physica C*, **471** (2011) 1167.

[18] Ueda S., Takeda S., Takano S., Mitsuda A. and Naito M., *Jpn. J. Appl. Phys.*, **51** (2012) 010103.

[19] Takeda S., Ueda S., Takano S., Yamamoto A. and Naito M., *Supercond. Sci. Technol.*, **25** (2012) 035007.

[20] Chuang T. M., Allan M. P., Lee J., Xie Y., Ni N., Bud'ko S. L., Boebinger G. S., Canfield P. C. and Davis J. C., *Science*, **327** (2010) 181.

[21] Grothe S., Chi S., Dosanjh P., Liang R., Hardy W. N., Burke S. A., Bonn D. A. and Pennec Y., *Phys. Rev. B*, **86** (2012) 174503.

[22] Guo Y., Zhang Y.-F., Bao X.-Y., Han T.-Z., Tang Z., Zhang L.-X., Zhu W.-G., Wang E. G., Niu Q., Qiu Z. Q., Jia J.-F., Zhao Z.-X. and Xue Q.-K., *Science*, **306** (2004) 1915.

[23] Özer M. M., Thompson J. R. and Weitering H. H., *Nat. Phys.*, **2** (2006) 173.

[24] Song C.-L., Wang Y.-L., Jiang Y.-P., Li Z., Wang L.-L., He K., Chen X., Ma X.-C. and Xue Q.-K., *Phys. Rev. B*, **84** (2011) 020503.

[25] Gooch M., Lv B., Tapp J. H., Tang Z., Lorenz B., Guloy A. M. and Chu P. C. W., *EPL*, **85** (2009) 27005.

[26] Zhang S. J., Wang X. C., Sammynaiken R., Tse J. S., Yang L. X., Li Z., Liu Q. Q., Desgreniers S., Yao Y., Liu H. Z. and Jin C. Q., *Phys. Rev. B*, **80** (2009) 014506.

[27] Sefat A. S., *Rep. Prog. Phys.*, **74** (2011) 124502.

[28] Wang Q.-Y., Li Z., Zhang W.-H., Zhang Z.-C., Zhang J.-S., Li W., Ding H., Ou Y.-B., Deng P., Chang K., Wen J., Song C.-L., He K., Jia J.-F., Ji S.-H., Wang Y.-Y., Wang L.-L., Chen X., Ma X.-C. and Xue Q.-K., *Chin. Phys. Lett.*, **29** (2012) 037402.

[29] He S., He J., Zhang W., Zhao L., Liu D., Liu X., Mou D., Ou Y.-B., Wang Q.-Y., Li Z., Wang L., Peng Y., Liu Y., Chen C., Yu L., Liu G., Dong X., Zhang J., Chen C., Xu Z., Chen X., Ma X., Xue Q. and Zhou X. J., *Nat. Mater.*, **12** (2013) 605.

[30] Tan S.-Y., Zhang Y., Xia M., Ye Z.-R., Chen F., Xie X., Peng R., Xu D.-F., Fan Q., Xu H.-C., Jiang J., Zhang T., Lai X.-C., Xiang T., Hu J.-P., Xie B.-P. and Feng D.-L., *Nat. Mater.*, **12** (2013) 634.

[31] Werthamer N. R., Helfand E. and Hohenberg P. C., *Phys. Rev.*, **147** (1966) 295.

[32] Cho K., Kim H., Tanatar M. A., Song Y. J., Kwon Y. S., Coniglio W. A. and Agosta C. C., *Phys. Rev. B*, **83** (2011) 060502.